energies

MDPI

Article

AIS-Based Estimation of Hydrogen Demand and Self-Sufficient Fuel Supply Systems for RoPax Ferries

Annika Christine Fitz [1,*], Juan Camilo Gómez Trillos [2] and Frank Sill Torres [3]

[1] German Aerospace Centre, Institute of Maritime Energy Systems, Max-Planck-Straße 2, 21502 Geesthacht, Germany
[2] German Aerospace Centre, Institute of Networked Energy Systems, Carl-von-Ossietzky-Straße 15, 26129 Oldenburg, Germany; juan.gomeztrillos@dlr.de
[3] German Aerospace Centre, Institute for the Protection of Maritime Infrastructures, Fischkai 1, 27572 Bremerhaven, Germany; frank.silltorres@dlr.de
* Correspondence: annika.fitz@dlr.de; Tel.: +49-4152-84881-18

Abstract: The International Maritime Organization (IMO) established new strategies that could lead to a significant reduction in the carbon footprint of the shipping sector to address global warming. A major factor in achieving this goal is transitioning to renewable fuels. This implies a challenge, as not only ship-innovative solutions but also a complete low-carbon fuel supply chain must be implemented. This work provides a method enabling the exploration of the potential of low-carbon fuel technologies for specific shipping routes up to larger sea regions. Several aspects including vessel sizes, impact of weather and shipping routes, emissions savings and costs are considered. The local energy use is determined with proven bottom-up prediction methods based on ship positioning data from the Automatic Identification System (AIS) in combination with weather and ship technical data. This methodology was extended by an approach to the generation of a basic low-carbon fuel system topology that enables the consideration of local demand profiles. The applicability of the proposed approach is discussed at hand via a case study on Roll-on/Roll-off passenger and cargo (RoPax) ferries transitioning from conventional fuels to a compressed hydrogen fuel system. The results indicate a potential reduction in emissions by up to 95% and possible system sizes and costs.

Keywords: emissions reduction; alternative marine fuels; hydrogen technologies; ship energy use estimation

Citation: Fitz, A.C.; Gómez Trillos, J.C.; Sill Torres, F. AIS-Based Estimation of Hydrogen Demand and Self-Sufficient Fuel Supply Systems for RoPax Ferries. *Energies* **2022**, *15*, 3482. https://doi.org/10.3390/en15103482

Academic Editors: Dheeraj Bharadwaj Gosala and Cody Michael Allen

Received: 30 March 2022
Accepted: 6 May 2022
Published: 10 May 2022

1. Introduction

The European Commission and the International Maritime Organization (IMO) adopted severe reduction targets in carbon dioxide (CO_2) emissions, which is a major greenhouse gas (GHG), for the marine sector [1,2]. Further substances such as nitrous oxides (NOx), sulfuric oxides (SOx) and particular matter (PM) are typical pollutants from diesel engine combustion [3]. They are associated with hazardous effects on the environment and human health [4].

Hence, the marine sector is facing the need to transition to cleaner low-carbon fuels, such as hydrogen, ammonia or methanol from renewable energy sources. While the targets are clear, the pathways to get there remain vague. Without reliable supply chains and systems, ship owners hesitate to order shipyards to construct ships with novel propulsion and fuel systems. Fuel producers and infrastructure providers, on the other hand, will not invest without predictable demand [5]. Pilot projects involving all stakeholders are required to demonstrate the feasibility of new fuel systems and attract further market players to invest.

Roll-on/roll-off passenger and cargo (RoPax) ferries can be identified as an attractive candidate for pilot projects. These types of ships carry passengers, cars and trucks mostly between two and sometimes among several different ports. Their stable location and

predictable energy demand reduce the uncertainty of integrating novel fuel systems. In the European market in 2019, 1396 operating RoPax vessels were registered. Ship sizes range from 30–240 m, from small river-crossing vessels up to super-ferries connecting international trading ports [6]. For 363 ships with a gross tonnage (gt) larger than 5000 t, a total fuel consumption of 4.4 Mt in 2019 was reported [7]. This accounts for 9% of the total marine fuel mass consumed in the EU [8].

The processing of ship positioning data from a ship's automatic identification system (AIS) is a common approach to estimate fuel consumption and related emissions and has been applied in various studies. The SHIP-DESMO model by Kristensen et al. estimates the energy use and ship emissions at different ship speeds based on a ship resistance model by Harvald (1983); missing ship technical data can be supplemented with statistical data [9]. In conjunction with AIS data, the model was used in an emissions inventory of the Arctic Sea by Winther et al. [10]. The STEAM model by Jalkanen et al. is based on ship resistance prediction methods presented by Hollenbach in 1998 and incorporates added resistance by sea conditions [11]. It was applied for emission inventories in the Baltic Sea in 2014 [12] and in European sea areas in 2016 [13]. On the largest scale, one can remark on studies carried out by the IMO on international waters, employing the propeller curve with constant values for weather effects and fouling in their Greenhouse Gas Studies from the years 2014 [14,15] and 2020 [15]. All listed methods are limited to analysis of the existing state and are not able to explore the potential of alternative fueling solutions.

General cost evaluations on utilizing hydrogen as an alternative energy carrier were performed by the Hydrogen Council, estimating the competitiveness in USD/km of transportation for RoPax ferries in the lower MW power range [16]. While this report provides a general indication of competitiveness, route and location-specific aspects, such as the specific operational and energy use profile or site-specific weather conditions, were not considered. Aarskog et al. presented an energy and cost analysis of a hydrogen-driven high-speed passenger ferry in Norway [17]. An AIS-based energy use profile and cost calculations were aligned with the installed equipment of the specific ship.

In this paper we provide a scheme that is able to consider ship and site-specific aspects and is also transferable to various locations and shipping routes. AIS-based methods are utilized to generate localized energy use profiles for RoPax ferries as an existing-state analysis incorporating the ship propeller curve model and weather conditions. The existing state of energy use is extended with an outlook on possible future setups utilizing low-carbon technology. A feasible low-carbon fuel system setup is generated based on the localized energy use profile. This allows for exploring the possibilities and benefits of transitioning to low-carbon technologies in terms of energy efficiency, emissions savings and system costs on a system component level. The explored scenarios were chosen to consider the whole supply chain, from renewable production to storage, distribution and end use, by estimating appropriate sizes of each system component. The generated fuel system scenario for a specific location may then support transparency and understanding in developing local synergetic systems.

This paper focuses on the use of compressed hydrogen systems. The method is generic and can be extended to other energy carriers. Figure 1 depicts the main components of a marine hydrogen fuel system that employs renewable resources. Here, a wind farm generates renewable energy, which feeds an electrolyser that produces hydrogen. The hydrogen is stored in an intermediate storage system and transported to the fuel station. At the fuel station, conditioned hydrogen is supplied to the RoPax vessels. The ships are equipped with a fuel cell propulsion system, generating electricity to supply an electric motor. As a typical setup, the fuel cell is combined with a battery in a hybrid configuration [18]. The option of landside charging of these ship batteries, likewise from the renewable energy source, is modeled.

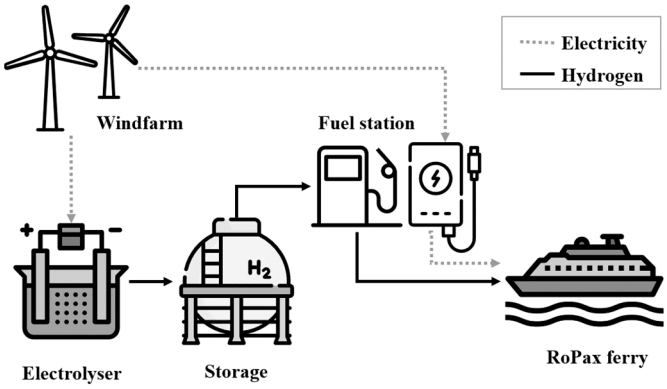

Figure 1. Marine hydrogen fuel system (Source: Created by author using Flaticon.com (accessed on 31 March 2021)).

The rest of this work is structured as follows. Section 2 presents the relevant methods of AIS energy use estimation as well as the state of technology for hydrogen fuel system components. In Section 3, the implementation of energy use estimation is presented, as well as the developed methodology for generating a low-carbon fuel system based on the localized energy use profile. Section 4 discusses a case study, and Section 5 concludes this work.

2. Preliminaries

This section describes the principles of AIS-based energy use estimation and the currently available technology relevant for marine hydrogen fuel systems.

2.1. Energy Use Prediction

The energy usage of ships can be determined by two different approaches, namely top-down and bottom-up methods. While top-down methods utilize measurements of consumed fuel quantities in retrospect to derive the energy use, bottom-up methods employ ship activity data, such as ship speed and weather conditions [18]. One advanced and equally common approach for tracking ship activity is recording and processing signals of the Automatic Identification System (AIS). AIS is a ship positioning data system, originally developed for collision prevention and made mandatory for passenger ships by the IMO [19]. Frequently exchanged messages among ships, terrestrial antennas and satellites contain information concerning the ship's speed, heading, draught and in some cases also further technical data such as ship dimensions, loaded cargo and destination [20].

The required propulsive power produced by the main engines P_{ME} can be estimated as a cubic function of ship speed v, commonly known as the propeller curve. The power is usually referenced to a power reference P_{ref} at a reference speed v_{ref}. It can be extended by considering the ship's ratio of actual to reference draught T/T_{ref} to the power of ⅔ as shown in Equation (1) [21].

$$P_{ME} = P_{ref} * \left(\frac{T}{T_{ref}}\right)^{\frac{2}{3}} * \left(\frac{v}{v_{ref}}\right)^{3} \quad (1)$$

In many cases, the installed main engine power $P_{ME,inst}$ will exceed P_{ref} due to safety or market availability reasons. Hence, it should be corrected with the downscaling factor ε_p as applied by Jalkanen to obtain P_{ref}, as depicted in Equation (2) [22].

$$P_{ref} = P_{ME,inst} * \varepsilon_p \quad (2)$$

The reference power P_{ref} applies in reference conditions, i.e., a steady-state movement in calm water, without wind, with a clean ship hull and great water depth [21]. In operational, real sea conditions, hull fouling, shallow waters and steering can all lead to higher

resistance. The added resistance can be expressed by the speed penalty $\Delta v/v$ [23]. Thus, the required propulsive power P can be stated according to Equation (3):

$$P_{ME} = \varepsilon_P * P_{ME,\,inst} * \left(\frac{T}{T_{ref}}\right)^{\frac{2}{3}} * \left(\frac{v * \left(1 + \frac{\Delta v}{v}\right)}{v_{ref}}\right)^3 \quad (3)$$

Next to the main engine delivering propulsive power, an auxiliary engine serves all further power needs P_{AE} such as on-board electricity or bow and stern thrusters.

Installed auxiliary power $P_{AE,\,inst}$ can be estimated as a proportion of $P_{ME,inst}$ and its load factor in operation LF_{AE} depending on the operating state (e.g., at berth, maneuvering, cruising), as shown by Equation (4).

$$P_{AE} = P_{AE,\,inst} * LF_{AE} \quad (4)$$

This approach was utilized by the United States Environmental Protection Agency (EPA) in 2010 [18]. Other approaches use fixed power values per operating states, e.g., IMO 2020 [15], or include the number of cabins for passenger ships, as in Jalkanen 2012 [11].

The total fuel consumption m_{fuel} is summed over n AIS operating points, recorded in varying time intervals Δt with the main engine power $P_{ME,n}$ and auxiliary engine power $P_{AE,n}$ at their instantaneous fuel oil consumptions $SFOC_{ME,n}$ and $SFOC_{AE,n}$ within a time interval Δt, as described in Equation (5).

$$m_{fuel} = \sum_{0}^{n} (P_{ME,n} * SFOC_{ME,n} + P_{AE,n} * SOFC_{AE,n}) * \Delta t \quad (5)$$

The specific fuel-oil consumption ($SFOC$) is the efficiency parameter of the main or auxiliary engine and depends on its type, model year, fuel type and exhaust aftertreatment system. Base values tabulated by the IMO are utilized and referred to as $SFOC_B$ [15]. Furthermore, $SFOC_B$ can be corrected to the load-specific fuel oil consumption $SFOC_L$ at different engine load factors LF [15]. The correction formula is here shown as Equation (6):

$$SFOC_L = SFOC_B * \left(0.455 * LF^2 - 0.71 * LF + 1.28\right) \quad (6)$$

The mass of combustion emissions m_p is calculated for the pollutants p (CO_2, NO_x, SO_x, $PM_{2.5}$) with Equation (5) and emission factors EF according to IMO GHG 2020 [15], employing Equation (7).

$$m_p = m_{fuel} * EF_p \quad (7)$$

2.2. Energy Supply with Hydrogen as Energy Carrier

Hydrogen is not an energy source per se but an energy carrier. Its supply chain consists of an energy source used for the production of hydrogen molecules, hydrogen production equipment, storage, transport, a fuel station and finally the propulsive system of the vessel, as shown in Figure 1. This section introduces different technology options for such a fuel sytem.

In order to reduce carbon emissions by utilizing hydrogen, the primary energy source must be low-carbon, such as wind or solar power. In this particular case only, hydrogen is denominated as 'green hydrogen' [24]. Most commonly, green hydrogen is produced by electrolysis, the splitting of water molecules between two electrodes with the addition of electric energy [25], i.e.,

$$H_2O \rightleftharpoons H_2 + 0.5\,O_2 \qquad \Delta H = +\frac{285.8\ \text{kJ}}{\text{mol}} \quad (8)$$

Different types of electrolysers are distinguished by their electrolyte. The commercially available types are polymer exchange membrane (PEM) and Alkaline [25]. In their current state, both types of technology achieve similar system sizes and costs [26].

Due to fluctuations in demand, the fuel system requires storage options that act as buffers. Low-pressure tanks and pipes can be utilized with pressure levels up to 100 bars [27]. For mobile applications, such as for transport in tube-trailers or the fuel tanks of vehicles with hydrogen propulsion systems, high-pressure vessels are utilized. Pressures of 200–700 bars are proven with metal containers and an increased proportion of composite materials, up to full composite vessels [28]. For liquified storage at ambient pressure, hydrogen needs to be cooled to its boiling point of −253 °C [29]. The cooling process is highly energy intensive, consuming approximately a third of the gravimetric energy density, compared to compression, which requires approximately a fifth [30], while the volumetric energy density is improved at low pressures. Other options, such as adsorption to porous materials, binding into metal hydrides or chemical storage in the form of methanol, ammonia or liquid organic hydrogen carriers, are under development [27].

For the transportation of hydrogen, the most efficient way is pipeline grids, as demonstrated in, e.g., the Ruhr area of Germany [31]. Conversions of natural gas pipelines are possible and targeted by the German government, but not yet widely available [24]. Transport by tube trailers in liquid or gaseous form can be utilized, as shown for on-road applications in Reddi 2014 [28] and Aliquo 2016 [32].

Fuel stations serve to dispense hydrogen to vessels at the target pressure and at safe temperatures. Multiple on-road stations have been realized [33] and can be used as a reference for the marine sector, in which hydrogen fueling is a novel technology. Compressors are a key component of the station, along with a cascaded high-pressure buffer storage, a cooling system and a dispensing system [28]. A major difference in marine applications is that the cascaded high-pressure storage may be omitted, as it serves to maintain a high pressure level for fueling multiple smaller tanks. In the piloting project HySeas III it was estimated that with a low rate of fuel events but large fuel volumes, cascaded buffer storage may be omitted and compensated for by a larger compressor [34]. Optionally, a hydrogen fuel station might also have charging facilities for battery and fuel cell hybrid propulsion systems. Battery charging of maritime vessels has been demonstrated for vessels of different sizes [35]. Electricity from the landside grid has to be converted based on the on-board electricity grid in terms of electric current magnitude, type (alternating or direct current) and voltage level [36].

The next component of the hydrogen fuel system is the fuel cell/battery hybrid ship system. The chemical energy stored in hydrogen is converted into electricity and used onboard for several purposes such as propulsion (after conversion to mechanical energy), electronic equipment and lighting, among others. In the on-road mobility market, fuel cells of the PEM type became the most dominant because of their quick start-up times, simple structure and improved transient performance for mobile applications. PEM fuel cells, running on green hydrogen, are among the cleanest combustion systems, as they minimize GHG emissions and the emittance of hazardous substances into their direct environment [37]. To achieve sufficient transient performance and full maneuverability of the ship, it is beneficial to combine the fuel cell with a battery in a hybrid system [38]. Most favorable are batteries using lithium-ion chemistry, which provides the most advantageous combination of energy density, possible charging and de-charging rates, and energy efficiency [39]. The efficient interaction of fuel cell and battery in the different operating states of the ship is controlled by an energy management system (EMS). EMS can be realized in various forms, such as rule-based and optimizing strategies [40]. The specific control strategy determines the final share of the energy supply contributed by each component in the energy system. A simplified depiction of a ship fuel cell hybrid system (without voltage and current conditioning) is shown in Figure 2 [41]. A battery (Bat) and PEM fuel cell (FC) feed into a common electricity bus, controlled by the EMS. The PEM fuel cell is fed from a hydrogen tank, the battery is charged and discharged from the shared electricity bus. From

the main bus, energy is supplied to the electric motor and propeller for the propulsion as well as to the secondary bus to supply auxiliary loads.

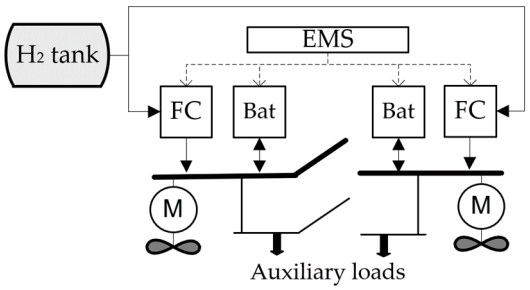

Figure 2. Fuel cell/battery hybrid propulsion system (Source: By author).

3. Materials and Methods

A fundamental contribution of this work is a solution that allows for a fast and location-specific exploration of a transition to sustainable modes of transportation. Therefore, a method is proposed that enables the transformation of an AIS-based energy demand profile into the energy demand profile of an alternative fuel system. A basic set of system topologies is presented to provide an estimation of possible system sizes, costs and seasonal behavior.

The methodology is divided into three sub-tasks: first, the analysis of the operational pattern of the ship, including its travel, landing and service break times; second, the energy use associated with the operational profile, applying technical data and local weather conditions; and third, the application of an alternative fuel system for the selected ship or sea region based on the previously analyzed operational profile and energy use.

3.1. Operational Analysis

AIS signals were filtered for the Maritime Mobile Service Identity (MMSI) numbers for single ships or fleets and time periods. Erroneous and missing signals were handled with filters and linear interpolation, depending on ship speeds and the length of the data gap.

Each operating point was assigned an operational state (at berth/anchored/maneuvering/slow cruising/cruising) depending on its speed, main engine load factor, and distance to the next port or coastline, according to Table 1.

Table 1. Classification of operating state according to vessel speed and distance to the next port.

Speed V	Main Engine Load Factor	Distance to Next Port	State
<1 kn	any	<3 km	at berth
		>3 km	anchored
1 < V > 5 kn	any	<3 km	maneuvering
		>3 km	open-water maneuvering
>5 kn	<0.65	any	slow cruising
	>0.65		cruising

In the last step, gridded atmospheric (wind speed, direction) and ocean data (wave height, direction, surface temperature) were merged per time and AIS position signal. The angle of attack of the ocean waves and the wind on the ship with its true heading were calculated using a 360° coordinate system with 0° referring to North, as utilized in [11].

The prepared data set allows for analysis of the typical operating profile of the ship, such as length of trips or time spent in port. Furthermore, relevant environmental conditions such as operating temperatures and exposure to wind and waves can be determined.

3.2. Energy Use Prediction

3.2.1. Ship Technical Parameters

For energy use prediction, ship technical parameters such as dimensions and motorization were required. Some parameters are mandatory; others can be replaced with statistical data, as shown in Appendix A, Table A1.

3.2.2. Speed Penalties

At each operating point, the speed penalty $\Delta v/v$ was calculated for the effects of ocean waves, wind, shallow waters and hull fouling. For the penalty of ocean waves $\Delta v/v_{sw}$ the model of Townsin and Kwon [42] was utilized with the formula for cargo ships and a block coefficient in the range of 0.55–0.7, considering the angle of attack of the ocean waves.

Added resistance by wind ΔR_W was calculated on the basis established by Blendermann, utilizing the drag coefficient profile for RoPax ships [43] and transposed to the wind speed penalty $\Delta v/v_w$ with the total expected resistance R_T based on Harvald [44] according to Equation (8) [23]:

$$\frac{\Delta v}{v}_{w} = \left(1 + \frac{\Delta R_W}{R_T}\right)^{\frac{1}{2}} - 1 \tag{9}$$

A shallow water speed penalty $\Delta v/v_{sh}$ was applied according to Lackenby [45] with an average expected water depth, especially relevant for channels and rivers.

Hull fouling was addressed with a constant factor of 0.18 on the ITTC-1957 hull friction coefficient [46], based on the findings of Aertssen [47], described in [23].

The speed penalty for hull fouling $\Delta v/v_f$ was obtained similarly to Equation (9). The total speed penalty $\Delta v/v$ is given by the total influence of waves, wind, shallow water and hull fouling:

$$\frac{\Delta v}{v} = \frac{\Delta v}{v}_{sw} + \frac{\Delta v}{v}_{w} + \frac{\Delta v}{v}_{sh} + \frac{\Delta v}{v}_{f} \tag{10}$$

3.2.3. Main Engine Power

The power output of the main engine was calculated for each operating point with Equation (3), considering the current ship draught (if provided by AIS data), ship speed and speed penalty due to real sea conditions. The installed engine power $P_{ME,\,inst}$ was scaled by ε_P to the reference power if information on appropiate scaling was available. Otherwise, $P_{ME,\,inst}$ was used as P_{ref}.

3.2.4. Auxiliary Engine Power

Installed auxiliary engine capacity $P_{AE,\,inst}$ was estimated with a factor of 0.278 in $P_{ME,\,inst}$, based on [48]. Load factors LF_{AE} per operating state, as used in Equation (4), were developed based on data from the MV Shapinsay, the basis vessel for HySeas III [34]. Values were differentiated between three different comfort classes depending on the onboard facilities, as shown in Appendix A, Table A2.

3.2.5. Total Fuel Consumption and Emissions

The total consumed fuel mass m_{fuel} and the emission masses m_p for each pollutant were calculated with Equations (5) and (7). Fuel and external costs could be derived using cost factors and the total masses.

3.3. Low-Carbon Technology Transition

The operational profile, energy use and local renewable energy potential were utilized for the sizing of fuel system components, ship propulsion system, fuel station, storage, electrolysis and wind farm, as shown in Figure 3. The CAPital EXpenditures (CAPEX) were derived from the sizes of the components and the OPerational EXpenditures (OPEX) and emissions from the demand-driven operation of the fuel system. Finally, the Levelized Costs

Of Transportation (LCOT) could be calculated. In the following, the different conversion steps for component sizing are described.

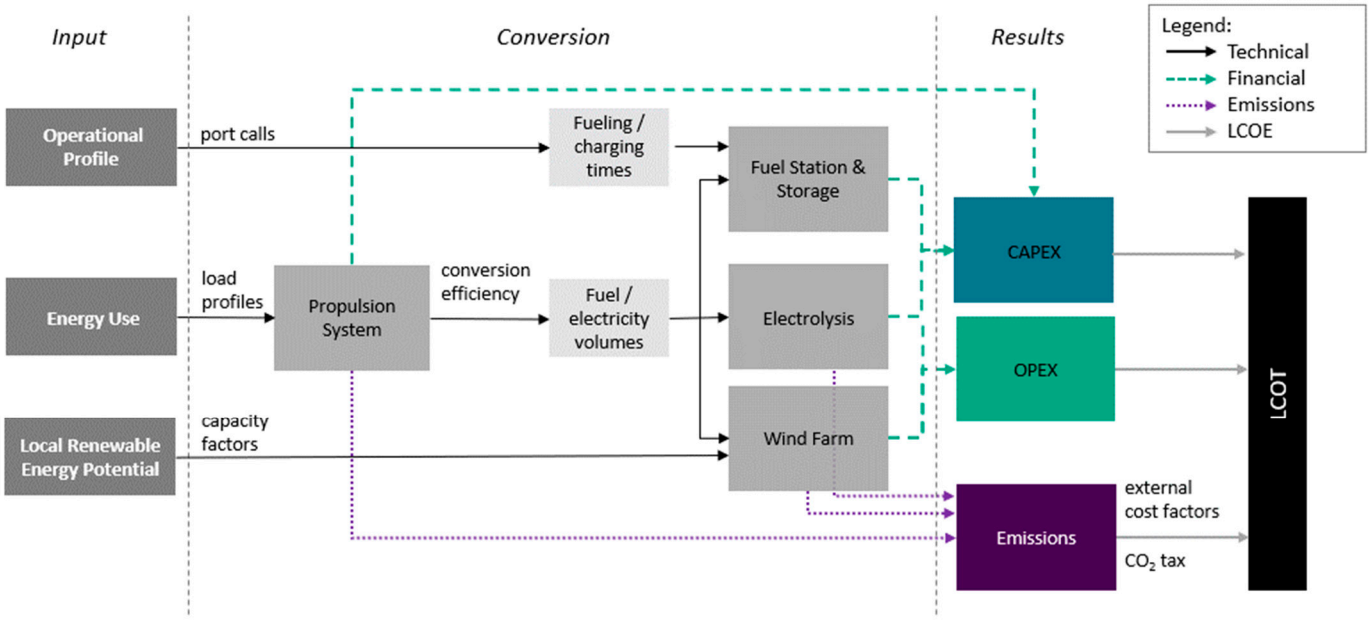

Figure 3. Transfer scheme for the operational profile and energy use of a RoPax ferry, as well as the renewable energy potential of a low-carbon fuel system (Source: By author).

3.3.1. Fuel Cell Hybrid Propulsion System

The fuel cell was sized such that it was able to deliver sufficient power for stable cruising at the ship's reference speed, i.e., to deliver P_{ref} at an appropriate fuel cell load factor $LF_{FCS,ref}$, according to Equation (11):

$$P_{FC} = \frac{P_{ref}}{LF_{FCS,ref}} \tag{11}$$

The necessary on-board energy storage was the maximum daily propulsive energy use $E_{P,daily,\ max}$. The designed (*des.*) energy storage of hydrogen $m_{H_2,\ des.}$ was derived using the degree of hybridization f_h, i.e., the energetic contribution of the battery to the propulsive energy depending on the EMS, as well as the fuel cell efficiency η_{FC} and lower heating value LHV_{H2}, according to Equation (12):

$$m_{H_2,\ des.} = \frac{E_{des.} * (1 - f_h)}{\eta_{FC} * LHV_{H2}} \tag{12}$$

The designed electric energy storage capacity $E_{E,des.}$ was calculated considering the discharge efficiency η_{B_d} and the minimum allowable state of charge (SOC_{min}) as shown in Equation (13):

$$E_{E,ds.} = \frac{E_{des.} * f_h}{\eta_{B_d}} * \left(1 + \frac{SOC_{min}}{(1 - SOC_{min})}\right) \tag{13}$$

3.3.2. Fuel Station

The hydrogen landside storage capacity m_{St} was the designed on-board capacity $m_{H_2,\ des.}$ multiplied by the days required for safe storage d_{St} as shown in Equation (14):

$$m_{St} = m_{H_2,\ des.} * d_{St} \tag{14}$$

The compressor power P_C (non-cascaded) was sized based on the required maximum fueling rate $\dot{m}$, according to fueling time restrictions and the minimum source pressure p_{min} of the hydrogen storage system, which could be a tube-trailer, low-pressure storage system or pipeline, as considered in Equation (15):

$$P_C = \dot{m} * \frac{1}{\eta_C} * T * \frac{k * R_{H_2}}{k-1} * \left[\frac{p_1}{p_{min}} - 1\right] \quad (15)$$

Which also required the compressor efficiency η_C, the source temperature T, the hydrogen specific heat relation k and the gas constant of hydrogen R_{H_2} as well as the on-board tank target pressure p_1.

If landside charging of the ship's battery was utilized, the required power P_{Ch} was aligned to the optimal battery charge rate (C-rate) $r_{c,opt}$:

$$P_{Ch} = E_{des.} * f_h * r_{c,opt} \quad (16)$$

With charging time restrictions, the C-rate could increase to a maximum of 1.

3.3.3. Electrolysis

The daily target production capacity $m_{H_2,\ EL,design}$ considered the buffering effect of the storage d_{St}. A rolling mean of d_{St} was applied to the daily hydrogen consumption and its maximum was $m_{H_2,\ EL,des.}$. This quantity was estimated using Equation (17):

$$m_{H_2,\ EL,des.} = \max\left(\frac{1}{d_s} * \sum_{i=1}^{d_{St}} m_{H_2,daily,i}\right) \quad (17)$$

Moreover, the required electrolyser power P_{EL}, based on the hydrogen higher heating value HHV_{H_2}, electrolyser efficiency η_{EL} and an average daily availability factor f_a, was calculated employing Equation (18):

$$P_{EL} = \frac{m_{H_2,EL,daily} * HHV_{H_2}}{\eta_{EL} * f_a * 24h} \quad (18)$$

3.3.4. Wind Farm

On a daily basis, the energy demand E_{tot} of the fuel station facilities and electrolyser had to be supplied by a wind farm operating at the local daily wind capacity factor C_W, according to Equation (19):

$$P_{W,req.,daily} = \frac{E_{tot}}{24\text{h} * C_W} \quad (19)$$

The capacity factor C_W was determined based on the daily wind speeds and a representative turbine model from the Python library windpowerlib [49].

The final size of the wind farm P_W was determined considering the buffer effect with a rolling mean of the window d_{St} over $P_{W,req.,daily}$. On a portion of r_{SS} days, representing the self-supply rate, the wind farm could provide the full energy. On a portion of $1 - r_{SS}$ days, grid electricity was added.

3.3.5. Levelized Costs of Transportation

For both systems, the base system and the alternative hydrogen system, levelized costs of transportation were calculated. The investment cost (CAPEX) and annual operating cost (OPEX) values of all system components were determined by cost factors, e.g., the nominal power of a component or the consumed fuel mass. The cost factors were determined based on literature research and industry interviews, as documented in Appendix A. Additionally, for the hydrogen-based system, excess energy from the wind farm was fed into the electricity grid, generating revenues R_E. The prices per kWh were determined by the average spot market and a supplemental renewable energy premium if applicable.

If a premium was part of the wind energy bidding process, e.g., as in Germany [50], an exponential decay ($e^{(-0.5)}$) of the premium was assumed, with a major drop in the next five years due to increasing competition.

Over the whole life span the LCOT were calculated using Equation (20):

$$\text{LCOT} = \frac{\sum_{t=1}^{lc} \text{CAPEX} + OPEX_t - R_{E,t}}{\sum_{t=1}^{lc} d_t} \quad (20)$$

including the life cycle length lc, investment cost CAPEX, annual operating cost $OPEX_t$, feed-in revenues $R_{E,t}$ and distance d_t. The cost of capital was neglected in the LCOTcalculation, as that relied on financial and political aspects, which are outside the scope of this model.

3.4. Implementation

The methodology was incorporated into a model coded in the open-source programming language Python, named 'ELS-Energy Lighthouse Software'. Due to company policies, the tool is only available for internal use.

4. Case Study

In a case study, the impact of using a hydrogen fuel system for two RoPax vessels was explored. These were the Earl Thorfinn, operating on various routes on the Orkney Islands, and the Frisia III, connecting the German island of Norderney with the mainland. The two ferries were selected due to the availability of fuel consumption data, allowing for the validation of the energy use estimation scheme. Furthermore, the sensitive natural environments of these ferries imply the use of alternative fuels in the future.

The analysis was conducted with a data basis of the year 2020, containing AIS tracking data, weather data, local wind energy capacities and ship technical data. Basic characteristics of the two vessels, as described in public web sources, are shown in Table 2.

Table 2. Ship technical data for the two case study vessels, including Maritime Mobile Service Identifier (MMSI) and basic dimensions.

	Unit	Earl Thorfinn	Frisia III
MMSI	-	232,000,760	211,692,820
Length	M	45.3	74.4
Breath	M	12.2	13.4
Gross Tonnage	Mt	771	1786
Speed	Kn	12	12
Power	kW	1486	1292
Passengers	-	191	1338
Lane-Meters	m	22	120

One can note that the installed capacity of the Earl Thorfinn exceeded that of the Frisia III, despite being a much smaller vessel, which can be ascribed to the harsher operating conditions on the Orkney Islands. Further parameters specific to the case study, as well as conversion factors utilized in the sizing and costs calculations, can be found in the full parameter set in Appendix A, Table A3.

4.1. Operational Analysis

First, the operation of the two vessels was analyzed, identifying their routes of operation, vessel speed, service patterns and typical times of port calls by tracking the AIS signals. Figure 4 shows one crossing of the Frisia III between its main port of Norddeich

and the island of Norderney. The speed profile over its course can be identified by the colors ranging from dark blue (at berth) to yellow (cruising speed).

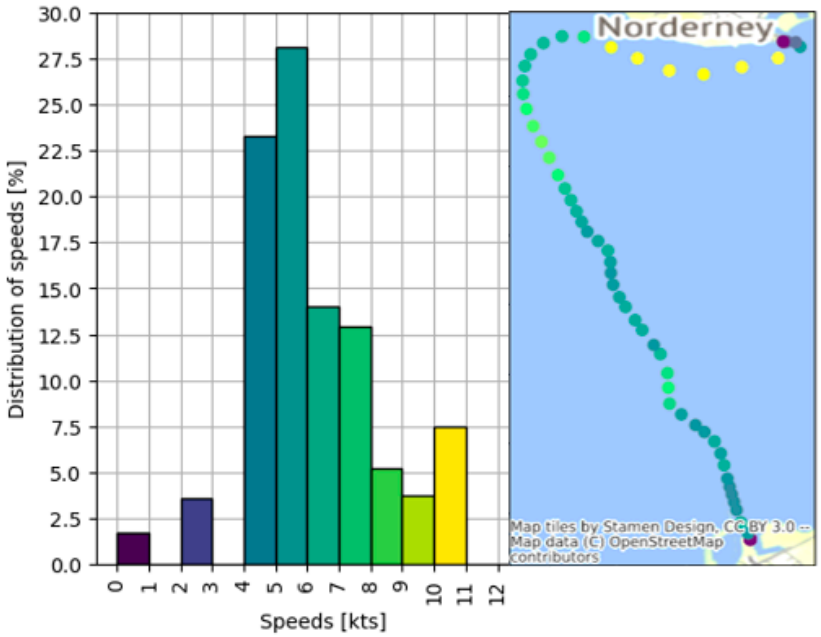

Figure 4. Speed profile and AIS tracking of one crossing by the Frisia III from Norddeich to Norderney. Note that more direct crossings are not possible due to the shallow waters of the Wadden Sea (Source: By author).

Longer or shorter time frames in the harbor are relevant for the available fueling time and for scaling the fueling station components. The port call times of each ship were identified based on the AIS data analysis, as presented in Table 3.

Table 3. Port call times of the two case study vessels, Earl Thorfinn and Frisia III, shown including breaks during operation and overnight.

Vessel	Earl Thorfinn	Frisia III
Main port	Kirkwall	Norddeich
Avg. port calls per day	1.37	4.53
Avg. time in port during operation [hh:mm]	02:51	00:48
Min. time in port outside operation [hh:mm]	09:42	13:10

One can note that the Earl Thorfinn has fewer calls in its main port per day as a result of traveling a longer route to multiple other island ports. The long port time during operation also indicates a possible fueling time slot during the day. The Frisia III, on the other hand, frequently calls at its main port with shorter port times during operation. Both ferries have long overnight stays in their main port, usable for charging or fueling.

In this study, therefore, a daily fueling and charging cycle was targeted. Alternatively, operating breaks could be utilized, especially for the Earl Thorfinn.

4.2. Energy Use Estimation

As described in Section 3.2, the ship speed, true heading, specific weather conditions and additional effects such as fouling and shallow waters were utilized to estimate the energy use.

AIS data were retrieved from AISHub.com (accessed on 31 March 2021) [51] and Lloyds Intelligence for the year of 2020. Weather data were added from the ERA 5 reanal-

ysis database of the European Centre for Medium-Range Weather Forecasts. A seabed topography model is not yet incorporated into the model. Therefore, an average water-depth of 5 m was assumed for the shallow waters of the Wadden Sea, relevant for energy use calculation for the Frisia III. Figure 5 depicts the daily energy use, with error bars presented based on the assumption of full AIS availability and no loss of signal. The standard deviation of the calculated propulsive power from the model is up to 18%, depending on errors in speed, wave and draught measurement and the specified reference power. The Earl Thorfinn showed higher variation in energy use, with typical values ranging from 1–3.5 t of diesel fuel per week, while the Frisia III averaged approximately 1.5 t/week. Longer periods out of operation could be noticed for the Frisia III as an effect of the COVID-19 pandemic and the associated lockdown measures in the year 2020. As the operation during the summer months, when the islands are most frequented, reached regular operation, data from the year 2020 are still suitable for sizing the production and storage capacities of a hydrogen fuel system. Nevertheless, this poses limitations regarding adapting to the seasonal variation. Over the full course of the year, the Frisia III reached slightly higher values in energy use and fuel consumption with 2328 MWh and 468 t, compared to the Earl Thorfinn with 2229 MWh and 430 t (see also Figure 5).

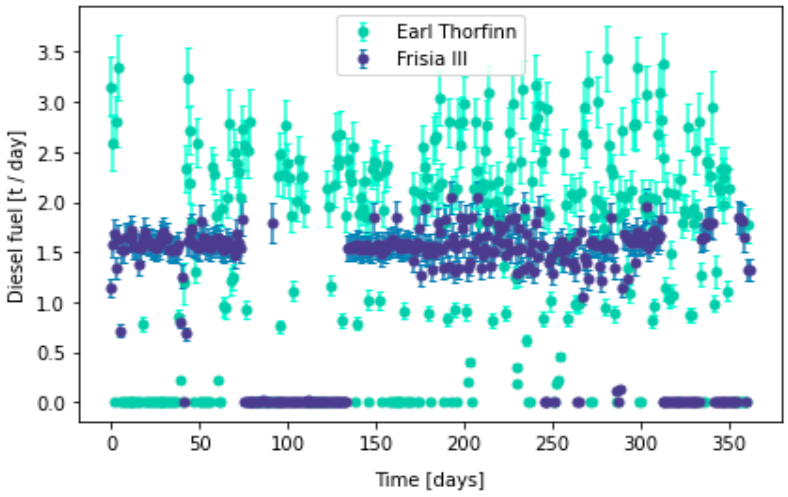

Figure 5. Fuel consumption, in tons per day, of the Earl Thorfinn and Frisia III in the year 2020 (Source: By author).

The estimated fuel consumption values were contrasted against real consumption data for both ships. In the case of the Earl Thorfinn, the estimated consumption was 91.8% of the real consumption, whereas for the Frisia III it exceeded real consumption by 2.1%. Therefore, the model underestimated consumption in the former case and overestimated it in the latter case. Major daily offsets for the Earl Thorfinn were caused by the loss of the AIS signal as a result of transceiver malfunction, signal blocking or insufficient coverage of the terrestrial antennas. Smaller gaps in AIS signals could be addressed by linear interpolation, while larger gaps distort the energy use profile. For future improvement, these gaps could be filled by replicating the typical operational profile per weekday. Further distortions could be observed on days of severe weather impact. This can be explained by the high sensitivity of ship propulsive power to wave height. Wave height data, obtained in this study from the ECMWF, were only available with a raster size of 55.5 km $\times$ 55.5 km. Therefore, local phenomena, especially in bays, might not be precisely represented. Further sources of bias may include imprecise ship technical data, deviations in the cubic relationship of power to speed due to specific vessel characteristics, and other environmental impacts such as ocean currents.

4.3. Hydrogen Fuel System

An alternative fuel system should be able to secure the required energy use of transportation throughout the year and with seasonal fluctuations. Local aspects were therefore considered while parameterizing the model. For instance, the offshore wind farm location north of Norderney was assumed to be the primary energy source in the Frisia scenario. For the Earl Thorfinn on the Orkneys, onshore energy installations were considered. Both scenarios use electrolysis in a demand-driven operation to produce hydrogen. For the Frisia III, it was chosen for electrolysis to be operated close to the harbor, feeding into a low-pressure storage system. For the Earl Thorfinn, hydrogen production was assumed to be off-site and transported via tube-trailers to the harbor over a range of <50 km.

4.3.1. System Sizing and Energy Balance

The fuel system components were sized using the basic scheme presented in Section 3. Conversion parameters of the individual fuel system components, such as efficiencies, hydrogen storage conditions, gravimetric and volumetric sizing factors, and cost factors, can be found in the case study-specific parameter set of Appendix A, Table A3. In Table 4, partial results are shown for the wind farm, electrolysis, buffer storage, compression unit and onboard hydrogen storage capacity.

Table 4. Partial results of hydrogen fuel system component sizing for the Earl Thorfinn and Frisia III.

Sizing Parameter	Earl Thorfinn	Frisia III
Wind farm capacity P_W [MW]	4.0	3.4
Electrolyser capacity P_{ELY} [MW]	2.21	1.7
Hydrogen fuel station gravimetric storage capacity m_{St} [kg]	1800	1246
Fueling compressor capacity P_C [MW]	0.75	1.25
Onboard hydrogen gravimetric capacity $m_{H_2,des.}$ [kg]	882	684

The required capacity of the windfarm was determined including a buffering effect of the hydrogen storage and based on the energy autonomy criteria of 80% of the days. Appendix B, Figure A1 indicates the required capacities for lower or higher self-supply rates. Appendix B, Figure A2 shows the balance of generated and used energy of the systems. Despite the similar annual energy use, as shown in Figure 5, the renewable source in the Orkney scenario requires higher capacities for the wind farm P_W, electrolysis system P_{ELY} and hydrogen storage system m_{St}. This is a result of the much higher fluctuations and higher daily peak energy use of the ship (see also Figure 5 and Appendix B, Figure A2). A more stable energy use profile, such as for the Frisia III, is beneficial for efficient sizing. For the compressor at the fuel station, the opposite can be observed. A much larger capacity is required as a result of the low source pressure, 50 bar, of the low-pressure hydrogen storage, as opposed to the 250 bar of the tube-trailer transport. Longer compression times at the electrolysis station compared to the hydrogen fueling time at the fuel station allow for an overall lower compression capacity. While both paths, tube-trailers combined with smaller compression capacity versus low-pressure storage with larger compression capacity, lead to sufficient fueling rates, the optimum configuration in each specific case will depend on the local availability of space as well as the distance between electrolyser and fueling station, which is outside the scope of this work.

In conclusion, it can be stated that the presented scheme allocates a sufficient energy source and fuel conversion system for a ship's energy use. For future work, the scheme could be extended by optimizing the size relations within the fuel conversion path.

4.3.2. CAPEX, OPEX and Wind Energy Revenues

The total investment costs of both systems differ significantly with 15.92 million EUR for the Earl Thorfinn compared to 26.25 million EUR for the Frisia III. The most significant

difference can be seen in the proportion of the wind farm costs within the total investment costs (Figure 6). Besides the wind farm, the remaining proportions of system costs were allocated similarly in both cases, with costs of the fuel cell system being dominant, followed by the costs of electrolysis and the fuel station system. The supplementary systems on board of the ship, such as the balancing battery, hydrogen tank, electrical grid and auxiliary systems, added up to approximately 60% of the costs of the fuel cell system.

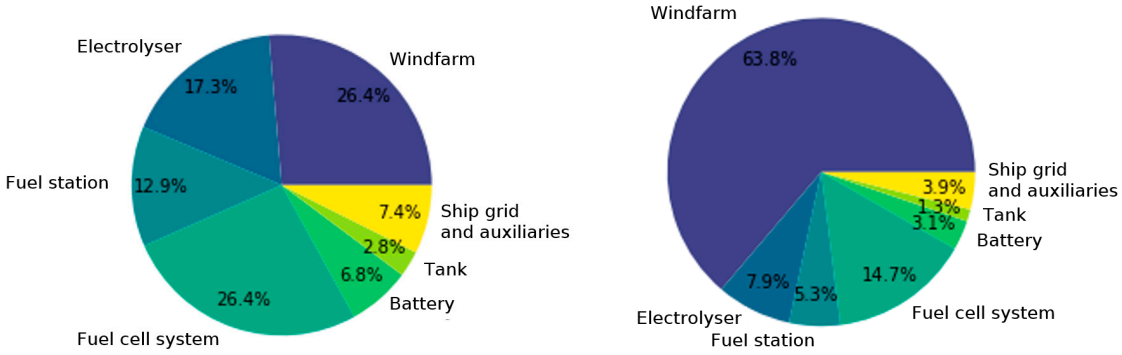

Figure 6. Estimated fuel system cost proportions: (**a**) Earl Thorfinn at a total CAPEX of 15.92 million EUR, (**b**) Frisia III at a total CAPEX of 26.25 million EUR (Source: By author).

The difference in the cost structure was mainly driven by the type of wind farm. The Orkney Islands allow for positioning of the wind turbines on land, thereby making up only a third of the cost of an offshore installation. Similar findings apply to the system maintenance costs, which were 0.26 million EUR per annum for case 1 and 0.61 million EUR for case 2, where offshore wind farm maintenance was the major driver in OPEX.

In both cases, the hydrogen production is initiated based on demand and follows the energy use profile with the buffering effect of the hydrogen storage system. Excess energy from the wind turbines is fed into the grid, while energy deficits on days of low wind capacity have to be supplemented by the grid. The annual balance of fuel system energy use, wind energy produced and traded grid quantities is shown in Table 5.

Table 5. Wind farm energy production versus actual fuel system energy use and resulting excess energy balance.

	Earl Thorfinn	**Frisia III**
Energy produced by wind farm [MWh/y]	18,474	20,164
Hydrogen fuel system total energy use [MWh/y]	7816	7943
Grid purchase [MWh/y]	1203	1053
Grid feed-in [MWh/y]	11,860	13,274
Excess wind energy revenues [M€/y]	+0.174	+0.254

With a decreasing wind premium scheme, such as in the case of Frisia III, the financial balance is only representative for the first year.

In both cases, the criteria of over 80% energy autonomy is met; however, a major portion of the produced energy is fed into the grid, achieving 42.3% and 39.4% self-consumption, respectively, of produced wind energy.

To increase self-consumption and the effective use of infrastructure, a larger hydrogen storage than the two-day buffer would be required. Furthermore, the interaction among available wind energy, electrolysis and current spot market price could be optimized by considering hourly instead of daily values, which is outside the scope of this work.

4.3.3. Emissions

Through implementing a hydrogen fuel system, the CO_2, NO_x, SO_x, and PM2.5 emissions and related external costs for both scenarios could be reduced significantly compared to the diesel base case, as shown in Table 6. The overall reduction in external emission costs was above 95% in both cases.

Table 6. Emission reductions through implementation of a hydrogen fuel system.

Scenario Parameter	Earl Thorfinn	Frisia III
Diesel use base [t/y]	430	468
CO_2 mass base [t/y], at 0.260 t€/t	1409.1	1463
NO_x mass base [t/y], at 12.6 t€/t	71.1	58.2
SO_x base [t/y], at 4.3 t€/t	0.6	0.7
$PM_{2.5}$ mass base [t/y], at 70.0 t€/t	1.0	1.1
Emission external costs [M€/y]	1.335	1.194
Expected CO_2 tax [M€/y]	0.035	0.037
Hydrogen use altern. [t/y]	111.7	114.1
CO_2 altern. [t/y], at 0.260 t€/t	211.0	214.4
Emission external costs [M€/y]	0.055	0.056
CO_2 tax altern. [M€/y]	0.005	0.005
Hydrogen fuel system external emission cost savings [%]	95.9%	95.3%
CO_2 tax savings [%]	85.7%	86.5%

Due to similar energy use, the emission levels of both ships remained comparable. The older combustion engine technology of the Earl Thorfinn leads to higher NO_x emissions and increased emissions costs compared to the Frisia III.

4.3.4. Levelized Costs of Transportation (LCOT)

By calculating the LCOT, investment as well as operational cost can be compared between the base and the alternative system over the whole lifespan. A typical life cycle basis of 20 years for maritime applications, for both the diesel base case and the alternative hydrogen system, was assumed. Figure 7a depicts the LCOT for both vessels in the base case as well as the hydrogen fuel system case. With external emissions costs, the overall LCOT of the base cases exceeded those of the hydrogen fuel systems. Without these costs, the overall LCOT were lower. For hydrogen cases, the costs of the wind farm could be compensated for by revenues from excess wind energy to a full or partial extension. For Frisia III, the LCOT of hydrogen did not reach a comparable level to the base case.

For comparison, the fuel system was calculated without including a wind farm utilizing grid energy at an average price of 10 ct/kWh, as shown in Figure 7b.

The comparison of LCOT between a full hydrogen fuel system (see Figure 7a) and an approach utilizing grid electricity (Figure 7b) demonstrates a financial benefit from including a wind farm in the local energy system. This coincides with the expectation of a synergetic effect due to balancing wind energy fluctuations with hydrogen storage. On the other hand, it can be seen that hydrogen fuel systems cannot be financially competitive with conventional fueling with diesel on a full or partial system approach. However, further optimization of the system configuration may decrease the LCOT of the hydrogen system.

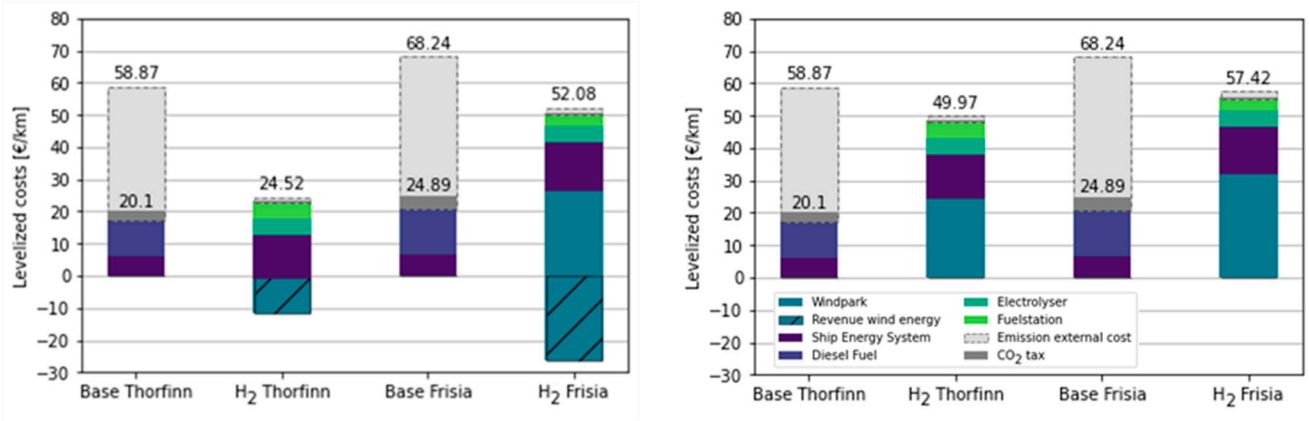

Figure 7. LCOT of a hydrogen fuel system, (**a**) including wind farm, electrolysis, storage, fueling system and fuel cell propulsion system, (**b**) without wind farm and using grid electricity for hydrogen production at 10 ct/kWh (Source: By author).

Autonomous fuel production and supply, including the wind farm, electrolyser and fuel station, exceeded the costs of diesel fuel sourcing. As already reflected in the system CAPEX (see Section 4.3.2), the wind farm was a major driver for LCOT as well, especially if an offshore application was utilized. Still, in the hydrogen scenario for the Earl Thorfinn, the high wind farm CAPEX could be compensated for by selling excess wind energy to the grid.

For the ship propulsion system, including the fuel cell, fuel tank, battery and auxiliaries, LCOT tripled compared to the base case due to higher component costs. However, the component costs were applied at the level of the year 2020 and might decrease with further market penetration and scale of production.

In terms of emissions for both vessels, the hydrogen fuel systems brought major benefits in LCOT. However, the full external emissions costs are not covered by the operator; only the CO_2 taxes are. Applying a linearly increasing price range of 25–125 EUR/t, CO_2 taxes cover only a small extent of the actual external costs and have little effect on the overall LCOT.

5. Conclusions

Because of their operation on stable routes, RoPax ferries are one of the vessel types predestined for the integration of novel low-carbon technologies. In this research, a combined method for operational profile analysis, energy use prediction and low-carbon fuel system transition modeling was developed, allowing for a fast assessment of routes or sea regions.

The methodology was tested on a case study of two appropriate vessels with the following findings. Ship tracking using AIS data, as also employed in other studies, was a robust and highly effective method for ship operational analysis, given sufficient availability of signals. The energy use prediction scheme from Jalkanen's model STEAM I [16], extended with the effects of wind, hull fouling and shallow waters, was identified as the most effective within the scope of the research. The standard deviation of the calculated propulsive power of the model was up to 18%, depending on errors in speed, wave and draught measurement and the specified reference power. Upon applying the scheme on two case study vessels, the predicted energy use was within ±10% of the actual annual use. The energy use profile was used to model an alternative hydrogen-fueled system. For both ships, savings in emissions external costs on the order of 95% and savings in CO_2 taxes above 85% could be achieved, leading to decreases in the levelized costs of transportation (LCOT) of 58% and 24%, respectively, when considering external emission costs of the CO_2, NO_X, SO_X and $PM_{2.5}$ exhaust gas emissions. However, on a system cost basis only (not

considering external emission costs and only CO_2 taxes), hydrogen-fueled systems at the current state of technology were more expensive, though the price increase tremendously depended on the specific installation possibilities and renewable energy potential on site.

In the scenarios, only wind power was used as a renewable energy source, which in both locations generated energy deficits in the summer months. For further investigations, this indicates the possibility of utilizing photovoltaic installations as a complementary energy source.

Integrating further vessel types that are relevant for renewable fueling will allow for modeling of hydrogen demand and supply systems containing various ship types to cover full sea regions, and for demonstrating the scalability of the tool.

Furthermore, the model may be extended by including operation on rivers, bathymetry maps of water depths, and consideration of currents. Additionally, the integration of other low-carbon fuels and renewable energy sources, as well as the integration of an excess energy-driven approach, should be pursued. The developed tool ELS, which implements the proposed methodology, allows for the assessment of single ship routes or ship fleets, the outlining of pathways to more sustainable fuel systems with different scenario options, and the indication of local hydrogen demands.

Consequently, the presented methodology is able to support the decision process regarding pioneering future marine fuel systems in an appropriate manner.

Author Contributions: Conceptualization, J.C.G.T. and F.S.T.; methodology, A.C.F.; software, A.C.F.; validation, A.C.F.; formal analysis, A.C.F.; investigation, A.C.F. and J.C.G.T.; resources, F.S.T.; data curation, A.C.F.; writing—original draft preparation, A.C.F.; writing—review and editing, J.C.G.T. and F.S.T.; visualization, A.C.F.; supervision, F.S.T. and J.C.G.T.; project administration, F.S.T. and J.C.G.T. All authors have read and agreed to the published version of the manuscript.

Funding: This research received no external funding.

Institutional Review Board Statement: Not applicable.

Informed Consent Statement: Not applicable.

Data Availability Statement: Not applicable.

Acknowledgments: The authors would like to thank Reederei Frisia and Orkney Island Council—Ferry Services for their contributions of data for the validation of the methodology.

Conflicts of Interest: The authors declare no conflict of interest.

Appendix A

Table A1. Ship technical data required for energy use evaluation and replacement parameters that can be utilized if data are missing. Statistical values are determined based on data collected from RoPax ferries by Kristensen et al. in 2016 [52].

Ship Technical Parameter	Missing Parameter Replacement
MMSI	Mandatory parameters
Length overall	
Breath	
Gross tonnage	
Dead weight, reference	
Draught, reference	
Ship speed, reference	
Main engine power, reference	

Table A1. *Cont.*

Ship Technical Parameter	Missing Parameter Replacement
Main engine type (slow/medium/high-speed)	Medium-speed diesel
ME model year	2000
ME fuel type	Heavy fuel oil
AE power	statistical
AE type	Medium-speed diesel
AE model year	2000
AE fuel type	Marine distillate oil
Midship section	statistical

Table A2. Ship comfort class classification and resulting auxiliary engine load factors in different states of operation.

Ship Facilities	Comfort Class	At Berth	Ma-Noeuvre	Slow Cruising	Cruising
Seating area without service	low	0.46	0.67	0.55	0.28
Seating area with service	medium	0.535	9.745	0.625	0.38 (+10%)
Hoteling facilities	high	0.61	0.82	0.7	0.48 (+20%)

Table A3. Specific parameter set for the case study, presented in this paper, with sources or explanations for the values chosen.

	Parameter	Unit	Value	Source/Basis
Emission external costs factors				
CO_2	c_{CO_2}	EUR/t	260	German Environmental Agency 2014 [53]. Medium long-term scenario (until 2050).
NO_x	c_{NOx}	EUR/t	12,600	TU Delft 2018 [4] Value for rural areas, as ships spend most of their operation in open water.
PM 2.5	$c_{PM2.5}$	EUR/t	7000	
SO_x	c_{SOx}	EUR/t	4300	Sanabra 2014 [54], lowest sensitivity.
Fuel cell propulsion system				
Degree of hybridization	f_h	%	35	Aligned to Han 2014 [38]
Li-Ion battery charging efficiency	η_{B_c}	%	90	Valoen 2007 [55]
Li-Ion battery discharging efficiency	η_{B_d}	%	85	
Max. C-Rate discharge	$r_{d,max}$	-	1	Scenario assumption
Opt. C-Rate charge	$r_{c,opt}$	-	0.3	Scenario assumption
Fuel cell system efficiency	η_{FCS}	%	50	Van Biert 2016, PEM-Fuel cell [56]
Fuel cell load factor at reference speed	$LF_{FCS,ref}$	%	70	Scenario assumption. For optimum range of 40–60% [38], operation at medium speeds.
Hydrogen tank ambient temperature	T	K	300	Scenario assumption for regular ambient temperature
Hydrogen tank pressure	p	bar	600	Current on-road technology Rivard 2019, Table 3 [57]
Compressibility factor at storage conditions	Z_{H_2}	-	1.38	Cengel 2008 [58]

Table A3. *Cont.*

	Parameter	Unit	Value	Source/Basis
Lowest allowable hydrogen tank pressure	$p_{H_2,min}$	bar	30	Similar empty tank pressure levels were used in HySeas III [34] and for the modeling of an on-road fueling station by Reddi in 2014 [28].
Battery min. allowable SOC	SOC_{min}	%	30	Scenario assumption for optimum battery lifetime
Battery vol. energy density	$\rho_{E,V}$	kWh/l	0.3	University of Washington 2020 [39]
Battery grav. energy density	$\rho_{E,m}$	kWh/kg	0.17	
Fuel cell cost factor	c_{FCS}	€/kW	1006	Estimate based on HySeas III project [34]
Hydrogen tank cost factor	c_{FT}	€/kg	519	Current on-road technology Rivard 2019, Table 3 [57]
Li-Ion battery cost factor	c_B	€/kWh	266.5	Cole 2021 [59]
Electric motor cost factor	c_{EM}	€/kW	10.25	Lipman 1999 [60]
Installation cost factor	c_i	%	20	Scenario assumption
Fuel Station				
Tube trailer capacity	m_T	kg	600	Aliquo 2016 [32]
Days of storage safety	d_S	d	2	Scenario assumption
Trailer cost factor per tank capacity	c_T	€/kg	500	Aliquo 2016 [32]
Max. pressure tube trailer	$p_{T,max}$	bars	250	
Min. pressure tube trailer	$p_{T,min}$	bars	30	Similar empty tank pressure levels were used in HySeas III and for the modeling of an on-road fueling station by Reddi in 2014 [28,34]
Max. pressure low-pressure storage	$p_{S,max}$	bars	50	Andersson 2019 [27]
Min. pressure low-pressure storage	$p_{S,min}$	bars	10	Scenario assumption
Low-pressure storage cost	c_S	€/kg	520	Parks 2014 [61]
Hydrogen grid pressure	p_g	bars	100	Scenario assumption
Max. flow rate per dispenser	$\dot{m}_{disp.}$	kg/s	0.05	HySeas III project [34]
Compressor isentropic efficiency	η_C	%	80	Parks 2014 [61]
Hydrogen source pressure	p_0	bars		Dependent on storage type.
Hydrogen target pressure	p_1	bars	650	Hydrogen ship tank pressure +50 bars
Compressor cos ts based on flow rate $\dot{m}$	C_C	€	$0.024283 * \dot{m}^{0.5202}$	Weinert 2005 [62]
Cooling temperature	T_C	K	253	Cooling level model for an on-road fueling station by Reddi in 2014 [28].
Cooler coefficient of performance	COP	%	90	Cengel 2008 [58]
Charging facility cost factor	c_{Ch}	€/kW	205	Nicholas 2018 [63]
Fuel Station OPEX factor	o_{FS}	%CAPEX/y	1	Scenario assumption.
Fuel station auxiliary systems energy use factor	e_{FS}	%	10	Scenario assumption.
Electrolysis station				
PEM Electrolyser efficiency	η_{EL}	%	80	Kumar 2019 [64] for PEM electrolyser, comparative 70% for Alkaline
Electrolyser availability	f_a	%	75	Scenario assumption.
Pressure after electrolysis	p_{EL}	bar	15	Scenario assumption.
Electrolysis auxiliary systems cost factor	f_{aux}	%	10	Scenario assumption.

Table A3. *Cont.*

	Parameter	Unit	Value	Source/Basis
OPEX factor	o_{EL}	%/y	1	Scenario assumption.
Electrolysis auxiliary systems energy use factor	e_{EL}	%	30	Scenario assumption for energy uses of water purification, temperature management
		Wind farm		
Days in buffer storage pipeline	d_b	d	5	Scenario assumption.
Minimum self-supply rate	r_{SS}	%	80	Scenario assumption.
Wind energy feed in spot price	t_{FI}	0.01 EUR/kWh	3.5	HySeas III project [34]
Offshore wind energy premium in Germany 2020	$t_{FI,premium}$	0.01 EUR/kWh	13.9	German Ministry of Economy and Climate Protection [50]
Grid electricity price	t_P	0.01 EUR/kWh	20	Scenario assumption.
Wind farm CAPEX factor	c_{WP}	EUR/kW	1237/ 4100	On-shore Stehly 2018 [65]/Off-shore Voormolen 2016 [66]
Wind farm OPEX factor	o_{WP}	EUR/kW/y	37/ 109	On-shore Stehly 2018 [65]/Off-shore Voormolen 2016 [66]
CO_2 emissions factor for wind energy	$EF_{CO_2,WE}$	g/kWh	27	Thomson 2015 [67]

Appendix B

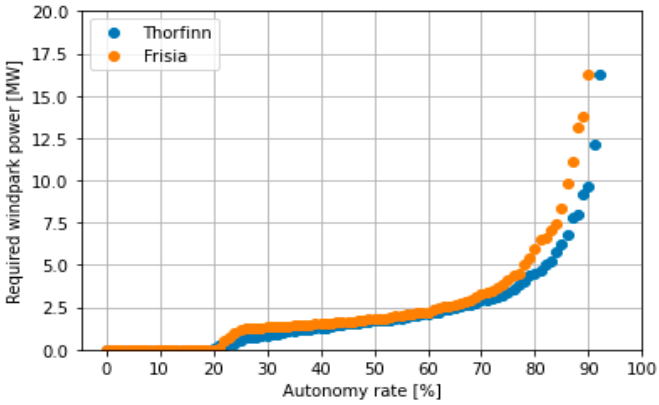

Figure A1. Required wind farm size at different rates of fuel system autonomy, meaning the proportion of days the system is able to generate enough energy for fuel production.

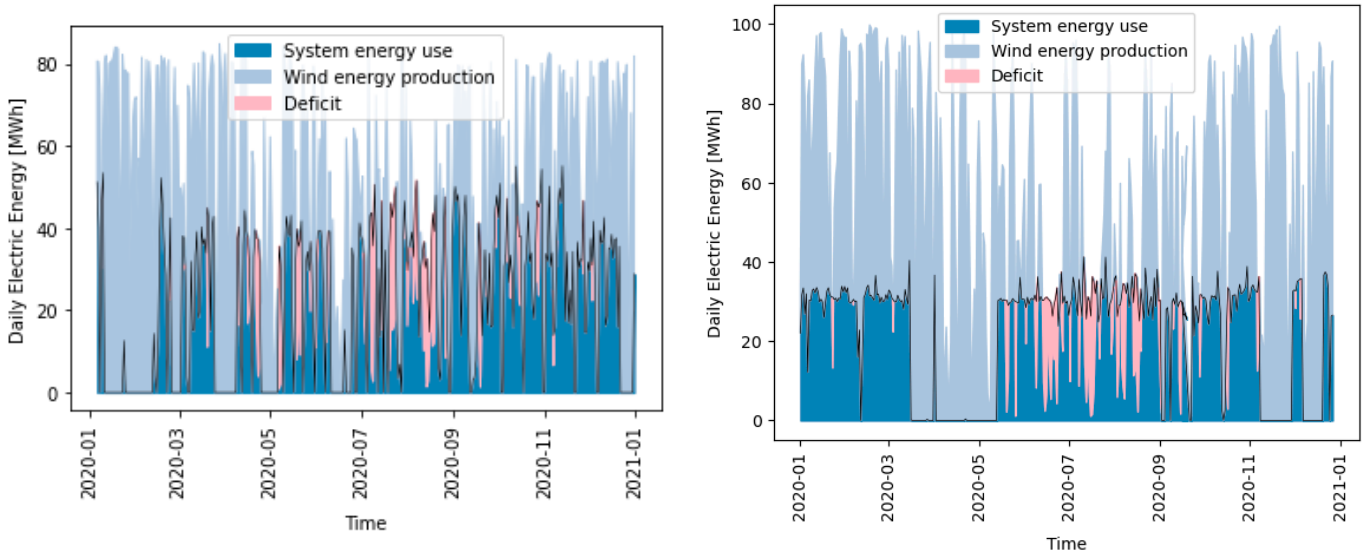

Figure A2. Hydrogen fuel system energy use and wind energy generation under the parameter set of Appendix A, Table A3, for the (**a**) Earl Thorfinn and (**b**) Frisia III.

References

1. European Commission. *Roadmap to A Single European Transport Area—Towards a Competitive and Resource Efficient Transport System*; COM(2011) 144 Final; European Commission: Brussels, Belgium, 2011; Available online: https://eur-lex.europa.eu/LexUriServ/LexUriServ.do?uri=COM:2011:0144:FIN:en:PDF (accessed on 5 May 2022).
2. International Maritime Organization (IMO). *Initial IMO Strategy on Reduction of GHG Emissions from Ships*; MEPC.304(72): London, UK, 13 April 2018; Available online: https://unfccc.int/sites/default/files/resource/250_IMO%20submission_Talanoa%20Dialogue_April%202018.pdf (accessed on 5 May 2022).
3. Reşitoğlu, İ.A.; Altinişik, K.; Keskin, A. The pollutant emissions from diesel-engine vehicles and exhaust aftertreatment systems. *Clean Technol. Environ. Policy* **2015**, *17*, 15–27. [CrossRef]
4. Hoen, A.; Nieuwenhuijse, I.; de Bruyn, S. *Health Impacts and Costs of Diesel Emissions in the EU*; CE Delft: Delft, The Netherlands, 2018; Available online: https://cedelft.eu/publications/health-impacts-and-costs-of-diesel-emissions-in-the-eu/ (accessed on 5 May 2022).
5. Petrospot Ltd. Session 4: Supply chain stakeholders have their say on the energy transition. In Proceedings of the Ship Energy Summit, Online. 8 September 2021.
6. Gómez Trillos, J.C. *HySeas III—Market Potential Analysis of RoPax Ferry Market in Europe*; Ref. Ares (2019)7435585; German Aerospace Centre (DLR): Oldenburg, Germany, 2019.
7. European Commission. THETIS-MRV CO_2 Emission Report. Available online: https://mrv.emsa.europa.eu/#public/emission-report (accessed on 1 November 2020).
8. Cooper, J. *Fuels Europe—Statistical Report 2019*; FuelsEurope: Brussels, Belgium, 2019; Available online: https://www.fuelseurope.eu/publication/statistical-report-2019/ (accessed on 5 May 2022).
9. Kristensen, H.O.; Psaraftis, H. Energy Demand and Exhaust Gas Emissions of Marine Engines. 2015. Available online: https://www.danishshipping.dk/en/services/beregningsvaerktoejer/download/Basic_Model_Linkarea_Link/806/energy-demand-and-emissions-of-marine-engines-september-2015.pdf (accessed on 5 May 2022).
10. Winther, M.; Christensen, J.H.; Plejdrup, M.S.; Ravn, E.S.; Eriksson, F.; Kristensen, H.O. Emission inventories for ships in the arctic based on satellite sampled AIS data. *Atmos. Environ.* **2014**, *91*, 1–14. [CrossRef]
11. Jalkanen, J.-P.; Johansson, L.; Kukkonen, J.; Brink, A.; Kalli, J.; Stipa, T. Extension of an assessment model of ship traffic exhaust emissions for particulate matter and carbon monoxide. *Atmos. Chem. Phys.* **2012**, *12*, 2641–2659. [CrossRef]
12. Jalkanen, J.-P.; Johansson, L.; Kukkonen, J. A comprehensive inventory of the ship traffic exhaust emissions in the Baltic Sea from 2006 to 2009. *Ambio* **2014**, *43*, 311–324. [CrossRef]
13. Jalkanen, J.-P.; Johansson, L.; Kukkonen, J. A comprehensive inventory of ship traffic exhaust emissions in the European sea areas in 2011. *Atmos. Chem. Phys.* **2016**, *16*, 71–84. [CrossRef]
14. International Maritime Organization (IMO). Third IMO Greenhouse Gas Study. 2014. Available online: https://www.imo.org/en/OurWork/Environment/Pages/Greenhouse-Gas-Studies-2014.aspx (accessed on 5 May 2022).
15. International Maritime Organization (IMO). Fourth IMO Greenhouse Gas Study. 2020. Available online: https://www.imo.org/en/OurWork/Environment/Pages/Fourth-IMO-Greenhouse-Gas-Study-2020.aspx (accessed on 9 April 2022).

16. Hydrogen Council. Path to Hydrogen Competitiveness—A Cost Perspective. 2020. Available online: https://hydrogencouncil.com/wp-content/uploads/2020/01/Path-to-Hydrogen-Competitiveness_Full-Study-1.pdf (accessed on 31 March 2021).
17. Aarskog, F.G.; Danebergs, J.; Strømgren, T.; Ulleberg, Ø. Energy and cost analysis of a hydrogen driven high speed passenger ferry. *Int. Shipbuild. Prog.* **2020**, *67*, 97–123. [CrossRef]
18. Waldron Davies, C.; Harnisch, J.; Oswaldo, L.; Mckibbon, S.; Saile, S.; Wagner, F.; Walsh, M. *2006 IPCC Guidelines for National Greenhouse Gas Inventories*; IPCC: Geneva, Switzerland, 2006.
19. Regulations for Carriage of AIS. International Maritime Organization (IMO). Available online: https://www.imo.org/en/OurWork/Safety/Pages/AIS.aspx (accessed on 3 March 2020).
20. Anwar, N. *Navigation Advanced Mates, Masters*, 1st ed.; Seamanship International: Lanarkshire, UK, 2006.
21. MAN Energy Solutions. *Basic Principles of Ship Propulsion*; MAN Energy Solutions: Copenhagen, Denmark, 2018; Available online: https://www.man-es.com/docs/default-source/marine/tools/basic-principles-of-ship-propulsion_web_links.pdf?sfvrsn=12d1b886_10 (accessed on 5 May 2022).
22. Jalkanen, J.-P.; Brink, A.; Kalli, J.; Pettersson, H.; Kukkonen, J.; Stipa, T. A modelling system for the exhaust emissions of marine traffic and its application in the Baltic Sea area. *Atmos. Chem. Phys.* **2009**, *9*, 9209–9223. [CrossRef]
23. Molland, A.F.; Turnock, S.R.; Hudson, D.A. *Ship Resistance and Propulsion: Practical Estimation of Ship Propulsive Power*, 2nd ed.; Cambridge University Press: Cambridge, UK, 2017.
24. German Federal Ministry for Economic Affairs and Energy. The National Hydrogen Strategy. 2020. Available online: https://www.bmwk.de/Redaktion/EN/Publikationen/Energie/the-national-hydrogen-strategy.pdf?__blob=publicationFile&v=6 (accessed on 5 May 2022).
25. Dincer, I. Green methods for hydrogen production. *Int. J. Hydrogen Energy* **2012**, *37*, 1954–1971. [CrossRef]
26. Thema, M.; Bauer, F.; Sterner, M. Power-to-Gas: Electrolysis and methanation status review. *Renew. Sustain. Energy Rev.* **2019**, *112*, 775–787. [CrossRef]
27. Andersson, J.; Grönkvist, S. Large-scale storage of hydrogen. *Int. J. Hydrogen Energy* **2019**, *44*, 11901–11919. [CrossRef]
28. Reddi, K.; Elgowainy, A.; Sutherland, E. Hydrogen refueling station compression and storage optimization with tube-trailer deliveries. *Int. J. Hydrogen Energy* **2014**, *39*, 19169–19181. [CrossRef]
29. Carriveau, R.; Ting, D.S.-K. (Eds.) *Methane and Hydrogen for Energy Storage*; Institution of Engineering and Technology: London, UK, 2016.
30. Elgowainy, A.; Wang, M.; Joseck, F.; Ward, J. Life-Cycle Analysis of Fuels and Vehicle Technologies. In *Encyclopedia of Sustainable Technologies*; Elsevier: Amsterdam, The Netherlands, 2017; pp. 317–327. [CrossRef]
31. German National Grid Agency. *Regulierung von Wasserstoffnetzen*; German National Grid Agency: Bonn, Germany, 2020; Available online: https://www.bundesnetzagentur.de/SharedDocs/Downloads/DE/Sachgebiete/Energie/Unternehmen_Institutionen/NetzentwicklungUndSmartGrid/Wasserstoff/Konsultationsbericht.pdf?__blob=publicationFile&v=1 (accessed on 5 May 2022).
32. Aliquo, J. Advanced Hydrogen Fueling Station Supply: Tube Trailers; U.S. Department of Energy. 2016. Available online: https://www.hydrogen.energy.gov/pdfs/review16/tv028_aliquo_2016_p.pdf (accessed on 31 March 2021).
33. Iwan, N. Network Expansion. Available online: https://h2.live/en/ (accessed on 31 March 2021).
34. Gómez Trillos, J.C. *HySeas III—Written Comunication with Project Personnel*; German Aerospace Centre, Institute of Networked Energy Systems: Oldenburg, Germany, 2021.
35. Moore, R. Color Hybrid: Technology Behind the World's Largest Plug-In Hybrid Ferry. Available online: https://www.rivieramm.com/news-content-hub/news-content-hub/color-hybrid-technology-behind-the-worldrsquos-largest-plug-in-hybrid-ferry-56251 (accessed on 5 May 2022).
36. Tvete, H.A. *ReCharge. Analysis of Charging- and Shore Power Infrastructure in Norwegian ports*; Hg. v. Det Norske Veritas Germanischer Lloyd (DNV-GL): Oslo, Norway, 2017.
37. Hansson, J.; Månsson, S.; Brynolf, S.; Grahn, M. Alternative marine fuels: Prospects based on multi-criteria decision analysis involving Swedish stakeholders. *Biomass Bioenergy* **2019**, *126*, 159–173. [CrossRef]
38. Han, J.; Charpentier, J.-F.; Tang, T. An Energy Management System of a Fuel Cell/Battery Hybrid Boat. *Energies* **2014**, *7*, 2799–2820. [CrossRef]
39. University of Washington. Lithium-Ion Battery. Available online: https://www.cei.washington.edu/education/science-of-solar/battery-technology/ (accessed on 31 March 2021).
40. Tang, D.; Zio, E.; Yuan, Y.; Zhao, J.; Yan, X. The energy management and optimization strategy for fuel cell hybrid ships. In Proceedings of the 2017 2nd International Conference on System Reliability and Safety (ICSRS 2017), Milan, Italy, 20–22 December 2017; pp. 277–281.
41. De-Troya, J.J.; Álvarez, C.; Fernández-Garrido, C.; Carral, L. Analysing the possibilities of using fuel cells in ships. *Int. J. Hydrogen Energy* **2016**, *41*, 2853–2866. [CrossRef]
42. Townsin, R.L.; Kwon, Y.J. Approximate formulae for the speed loss due to added resistance in wind and waves. *R.I.N.A. Suppl. Pap.* **1983**, *125*, 199.
43. Blendermann, W. *Schiffsform und Windlast: Korrelations- und Regressionsanalyse von Windkanalmessungen am Modell*; TUHH Hamburg University of Technology: Hamburg, Germany, 1993. [CrossRef]
44. Harvald, S.A. (Ed.) *Resistance and Propulsion of Ships*; Wiley: New York, NY, USA, 1983.
45. Lackenby, H. The effect of shallow water on ship speed. *Nav. Eng. J.* **1964**, *76*, 21–26. [CrossRef]

46. Prohaska, C.W.; Acevedo, M.L.; Hugues, G.; Kinoshita, M.; Landweber, L.; Lap, A.J.W.; Wieghardt, K. Skin Friction and Turbulence Simulation. In Proceedings of the International Towing Tank Conference (ITTC), Madrid, Spain, 15–23 September 1957; p. 45.
47. Aertssen, G.; Sluys, M.F.V. Service performance and seakeeping trials on a large containership. *R. Inst. Nav. Archit. Trans.* **1972**, *114*, 429–447.
48. United States Environmental Protection Agency (EPA). *Proposal to Designate an Emission Control Area for Nitrogen Oxides, Sulfur Oxides and Particulate Matter*; Office of Transportation and Air Quality: Ann Arbor, MI, USA, 2010.
49. Haas, S.; Krien, U.; Schachler, B.; Bot, S.; kyri-petrou; Zeli, V.; Shivam, K.; Bosch, S. *Wind-Python/Windpowerlib*; Silent Improvements, Zenodo: Genève, Switzerland, 2021. [CrossRef]
50. Bundesministerium für Wirtschaft und Energie, EEG-Vergütung. Available online: https://www.erneuerbare-energien.de/EE/Navigation/DE/Technologien/Windenergie-auf-See/Finanzierung/EEG-Verguetung/eeg-verguetung.html (accessed on 2 December 2021).
51. AISHub. Available online: www.aishub.net (accessed on 31 March 2021).
52. Kristensen, H.O.; Psaraftis, H. Prediction of Resistance and Propulsion Power of Ro-Ro Ships. 2016. Available online: https://www.danishshipping.dk/en/services/beregningsvaerktoejer/download/Basic_Model_Linkarea_Link/163/wp-2-report-4-resistance-and-propulsion-power.pdf (accessed on 5 May 2022).
53. Burger, A. *Schätzung der Umweltkosten in den Bereichen Energie und Verkehr*; Umeltbundesamt: Dessau-Roßlau, Germany, 2014; Available online: https://www.umweltbundesamt.de/sites/default/files/medien/378/publikationen/hgp_umweltkosten_0.pdf (accessed on 5 May 2022).
54. Sanabra, M.C.; Santamaría, J.J.U.; De Osés, F.X.M. Manoeuvring and hotelling external costs: Enough for alternative energy sources? *Marit. Policy Manag.* **2014**, *41*, 42–60. [CrossRef]
55. Valøen, L.O.; Shoesmith, M.; Moli, E.-O. The Effect of PHEV and HEV Duty Cycles on Battery and Battery Pack Performance. In Proceedings of the PHEV 2007 Conference: Where the Grid Meets the Road, Winnipeg, MB, Canada, 1–2 November 2007.
56. van Biert, L.; Godjevac, M.; Visser, K.; Aravind, P.V. A review of fuel cell systems for maritime applications. *J. Power Sour.* **2016**, *327*, 345–364. [CrossRef]
57. Rivard, E.; Trudeau, M.; Zaghib, K. Hydrogen Storage for Mobility: A Review. *Materials* **2019**, *12*, 1973. [CrossRef]
58. Çengel, Y.A. *Thermodynamics: An Engineering Approach*; McGraw-Hill Higher Education: Boston, MA, USA, 2008.
59. Cole, W.; Frazier, A.W.; Augustine, C. *NREL/TP-6A20-79236*; Cost Projections for Utility-Scale Battery Storage: 2021 Update; National Renewable Energy Laboratory: Golden, CO, USA, 2021.
60. Lipman, T.E. *The Cost of Manufacturing Electric Vehicle Drivetrains*; California Air Resources Board: Davis, CA, USA, 1999.
61. Parks, G.; Boyd, R.; Cornish, J.; Remick, R. *Hydrogen Station Compression, Storage, and Dispensing Technical Status and Costs: Systems Integration*; National Renewable Energy Lab.: Golden, CO, USA, 2014. [CrossRef]
62. Weinert, J. *A Near-Term Economic Analysis of Hydrogen Fueling Stations*; Institute of Transportation Studies, University of California: Davis, CA, USA, 2005.
63. Nicholas, M.; Hall, D. *Lessons Learned on Early Electric Vehicle Fast-Charging Deployments*; International Council on Clean Transportation: Washington, DC, USA, 2018; pp. 7–26. Available online: https://theicct.org/sites/default/files/publications/ZEV_fast_charging_white_paper_final.pdf (accessed on 5 May 2022).
64. Kumar, S.S.; Himabindu, V. Hydrogen production by PEM water electrolysis—A review. *Mater. Sci. Energy Technol.* **2019**, *2*, 442–454. [CrossRef]
65. Stehly, T.J.; Beiter, P.C. *2018 Cost of Wind Energy Review*; National Renewable Energy Lab: Golden, CO, USA, 2020. Available online: https://www.nrel.gov/docs/fy20osti/74598.pdf (accessed on 5 May 2022).
66. Voormolen, J.; Junginger, H.; van Sark, W. Unravelling historical cost developments of offshore wind energy in Europe. *Energy Policy* **2016**, *88*, 435–444. [CrossRef]
67. Thomson, C.; Harrison, G. *Life Cycle Costs and Carbon Emissions of Offshore Wind Power*; ClimateXChange: Edinburgh, UK, 2015; Available online: http://www.climatexchange.org.uk/files/4014/3325/2377/Main_Report_-_Life_Cycle_Costs_and_Carbon_Emissions_of_Offshore_Wind_Power.pdf (accessed on 5 May 2022).